Influence of free water on the quasi-static and dynamic strength of concrete in confined compression tests

P. Forquin [a,*], K. Safa [b], G. Gary [b]

[a] Laboratoire de Physique et de Mécanique des matériaux, Université de Metz, 57045 Metz, France
[b] Laboratoire de Mécanique des Solides, Ecole Polytechnique, 91128 Palaiseau, France

ARTICLE INFO

ABSTRACT

The behaviour of concrete under high pressure and dynamic loadings is experimentally investigated in the present paper. The specimen is confined in a cylindrical elastic steel ring that insures a quasi-uniaxial strain state of loading. It is subjected to static and dynamic (with strain rates in the range from $1e-6/s$ to $200/s$) axial compressive loadings. Transverse gauges glued on the lateral surface of the ring allow for the measurement of the confining pressure so that the volumetric and the deviatoric response of the specimen can be computed. At high or intermediate strain rates, water saturated and dried specimens show strongly different results: i.e. a continuous increase of strength with pressure in dried specimens and a quasi nil strength enhancement in water-saturated specimens. This difference is not observed with quasi-static loadings. As explained through a basic poromechanics analysis, this dissimilarity is mainly attributed to an increase of pore pressure inside the saturated concrete during fast (quasi-static or dynamic) experiments.

© 2009 Elsevier Ltd. All rights reserved.

1. Introduction

The deviatoric strength (the deviatoric stress being defined as the difference between the maximal and minimal principle stresses) and the compaction law of concrete under hydrostatic pressure up to one thousand of MPa with strain rates of several hundreds per second need to be investigated for both military and civil applications. These applications are connected with the safety of buildings or structures (power plants, head-quarters, tanks of dangerous materials, dams…) regarding accidental or intentional extreme loadings such as ballistic impact, blasting, rock fall, plane crash or also earthquake. Various environmental conditions can be found, in particular, regarding the presence of water.

Quasi-static and dynamic compressive behaviour of dry or wet concretes has been already investigated for almost one century by means of uniaxial compression tests, triaxial compression tests and more recently by means of quasi-oedometric compression tests. Several results are listed below.

1.1. Influence of free water on the compressive strength of concretes (triaxial tests)

In the triaxial compression tests, a purely hydrostatic pressure is first applied to a cylindrical specimen by a fluid. Afterwards, an axial compression is added. The influence of both axial strain and confining pressure on the deviatoric stress, taken as the axial stress minus the lateral pressure applied by the fluid, is then observed. The tests have shown the ductility of concretes under strong confinement and the increase of the strength with pressure [3,20,22,24,25,34]. Recently, triaxial tests with confining pressures as high as 500 MPa have been performed on "real" concrete, where the average aggregates size is about 8 mm [27,33]. An increase of the strength with the mean normal stress has been observed as it was the case for microconcrete [6]. However, no information about the influence of the free water content was mentioned. A more recent study [12] has been done on dried cylindrical concrete specimens of 7 cm in diameter and 14 cm in length. Triaxial, proportional, and oedometric paths were used to explore the behaviour of the material, with confining pressures up to 0.85 GPa and a maximum axial stress of 1.6 GPa. The tests revealed an increase of the compaction process with the level of the deviatoric stress attributed to a granular rearrangement inside the matrix under the shear stress.

Tests at different levels of saturation under triaxial loadings with confining pressures up to 650 MPa revealed the importance of the free water content, where the saturated samples exhibited a perfectly plastic behaviour regardless to the confining pressure [31]. Dried specimens showed a continuously increasing strength with the raise of the confining pressure, while specimens with different saturation ratios showed behaviours between the saturated and dried ones.

1.2. Static and dynamic quasi-oedometric compression tests

Considering an impact on a concrete structure, three effects are generally reported [35]. The first one is a scabbing on the front face. It is made of conical cracks due to unconfined compression in the

* Corresponding author.
E-mail addresses: Pascal.Forquin@univ-metz.fr (P. Forquin), Safa@lms.polytechnique.fr (K. Safa), Gary@lms.polytechnique.fr (G. Gary).
URL: http://lmsX.polytechnique.fr/LMSX/ (G. Gary).

direction orthogonal to the projectile trajectory [9]. It is followed in the core (second effect) by a confinement zone mainly generated by the inertia of the surrounding material. Finally, (third effect) tensile loading occurs on the opposite face of the target producing, for instance, spalling in the case of slabs [21]. The dynamic uniaxial deformation test is representative of the state of stresses inside the confined zone, although describing a particular loading path. During a Quasi-Oedometric Compression (QOC) test, a cylindrical specimen tightly enclosed in a confinement vessel is axially compressed. As it tends to expand, both radial and axial stresses increase in the specimen. The test provides a reading of the strength of the material at different levels of the pressure.

Several experimental devices for quasi-oedometric compression were proposed by Bažant et al. [2], Burlion [4,5] and Gatuingt [15]. Burlion [5], for instance, developed an instrumented elastic steel vessel. Gatuingt [15] performed dynamic tests with cells made of steel or brass. Forquin et al. [8,10] proposed an analysis of the experimental data taking account of the shortening of specimen and of a possible plastic deformation of the confining cell. More recently, dynamic QOC tests performed with a Split Hopkinson Pressure Bar device were analysed applying the previous methodology [11]. The accuracy of the method and the influence of friction were specially discussed. However, the influence of strain rate and free water has not been clearly demonstrated yet.

In the present study, a SHPB (Split Hopkinson Pressure Bar) device is used for the dynamic loading (in the range of strain rates from 80 to 200/s). Static tests are carried out by means of a hydraulic press. Data processing considers the shortening and the axial displacement of the specimen relatively to the confining ring. The steel ring allows for exploring the behaviour of concrete under levels of lateral pressure up to 800 MPa.

2. General description of quasi-oedometric compression tests and methodology used to process experimental data

An accurate description of the SHPB device used for the dynamic quasi-oedometric compression tests and of the processing technique has already been reported in [11]. In the present work, several modifications and improvements were introduced concerning the experimental procedure and the processing of data. All the details are listed below.

2.1. Concrete specimens

Cylindrical specimens of microconcrete called "MB50" were machined in large blocks ($15 \times 25 \times 72$ cm^3) 40 days after the mix was poured into watertight plywood moulds. Specimens have a diameter varying from 28.8 to 28.9 mm and are 40 mm long. Specimen then easily fits between the bars of the SHPB device (80 mm in diameter). The length to diameter ratio of specimens (~4/3) is the result of a compromise. On the one hand, under dynamic loading, shorter specimen is required to insure a better homogeneity of mechanical fields within the specimen. On the other hand, in regard to the size of the granulates, the size of the specimen must be representative of the material. The composition of the "MB50" concrete is given in Table 1. The distribution of aggregates and the aggregates to cement ratio (4.46) has been designed to make it representative of a standard concrete but with a smaller grain size: the mean grain size is about 2 mm and the maximum grain size does not exceed 5 mm that makes this "microconcrete" very attractive to perform experiments with relatively small specimens that are convenient for conventional hydraulic machines or for SHPB (Split Hopkinson Pressure Bar) loading devices. This is the reason why this concrete has been already studied in the past under tensile loading [26,30]; triaxial loading [6] and dynamic quasi-oedometric compression tests [11,15]. Two sets of specimens are considered in this study:

Table 1
Composition of the "MB50" microconcrete.

Sand (kg/m^3)	1783
Cement (kg/m^3)	400
Water (kg/m^3)	200
Admixture (kg/m^3)	12
Water/cement	0.5
Sand/cement	4.46
Max grain size (mm)	5

dried and fully saturated ones. In order to avoid the dissolution of "portlandite" in water, all the samples were stored in water saturated with lime. Afterwards, "saturated" specimens were picked-up from water, and directly inserted in the cell. The specimens of the second set ("dried" specimens) were oven-dried at 102 °C. The loss of mass in percentage regularly checked during the process indicated that, throughout the 48 h oven-drying, a constant weight of the specimen has been achieved.

2.2. Steel ring, strain gauges location and plugs

A ring of high-strength steel (elastic limit about 1800 MPa) was used to perform the quasi-oedometric compression tests (Fig. 1). An internal diameter of 29.3 mm was selected to reduce as much as possible the gap between the specimen and the ring (about 0.2 mm). The outer diameter and the length of the ring were optimised by a series of numerical simulations: the outer diameter (60 mm) was chosen small enough to permit for a good sensitivity of the strain gauges placed on its outer surface and large enough to prevent any plastic strain within the ring for an internal pressure applied up to 1000 MPa. The height of the ring (45 mm) is slightly larger than that of the specimen to avoid its getting out of the ring during the test.

Six hoop strain gauges were glued onto the external surface of the metallic ring (Fig. 1b) and the strain was recorded through a data acquisition card (12 bits) with the time base set to 1 μs. As explained later (see the part concerning the processing of data), the two gauges located in the middle of the ring (named G1 and G2) are used to deduce the radial stress level within the specimen. The four others (G3 to G6) are located at a distance from the middle equal to 3/4 of the half-length of the ring. They are used to evaluate the barrelling of the ring, by comparison with the two central gauges. They also indirectly provide an evaluation of the difference in axial displacement between the specimen and the ring.

The specimen is compressed by means of 2 cylindrical plugs (Fig. 1a) of high-strength steel (its elastic limit, about 1800 MPa, is higher than the maximal level of axial stress reaches during the tests). The steel plugs have the same diameter than the concrete specimens (28.8 mm) and are 40 mm long.

2.3. Mounting procedure

A special procedure was set to align the ring, the sample and the two plugs. A device (Fig. 2) was especially designed to introduce the concrete specimen within the ring. First, the concrete sample was scotch taped to the upper plug. The concrete specimen was slowly introduced within the ring that had been previously partially filled by a bi-components epoxy resin named "Chrysor® C6120". During this stage, the interface product is slowly extruded so that the internal gap between the specimen and the ring is totally filled by the Chrysor®.

2.4. Brief description of the SHPB system used for the dynamic tests

24 h later, the interface product is hardened and the set made of the ring, the specimen and the two plugs can be safely handled. It is inserted between the two bars of a SHPB (Split Hopkinson Pressure Bar). The SHPB system used in this work and the correspondent
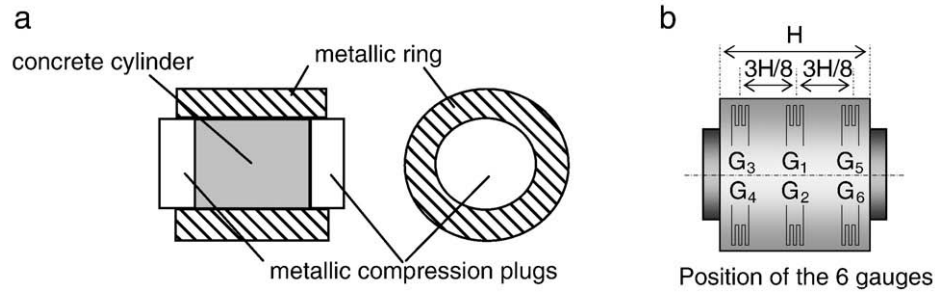
Fig. 1. Loading cell (a: left, b: right).

processing method was previously detailed in [11]. The SHPB set-up (striker, input bar and output bar) is made of steel (elastic limit 1200 MPa) with a diameter of 80 mm. The striker, the input bar and the output bar are 2.2 m, 6 m and 4 m long, respectively. Since our specimen is located between the two plugs, and not directly sandwiched between the input and output bars, forces and velocities have to be calculated at the faces of the specimen. Their calculation is based on the analysis of the wave propagations in a bar with a non constant acoustic impedance [1,13,14,23]. In the present (and simple) case there is only one impedance change, between the bar and the plug, both impedances being known. Knowing the basic waves, the waves at specimen faces are computed, allowing (with the same formulas as for the classical case) for the calculations of forces and displacements. As a brittle material is tested (at least at the early instants of the loading) it must be checked that the rising time of the loading is large enough to avoid failure before the stress equilibrium is attained. For this purpose, we use the so-called pulse-shaper technique. A thin disk of lead is put on the impact end of the input bar. As long as the lead is not totally flattened the maximum stress induced by the striker is not reached.

2.5. Method used to process the experimental data

A method was proposed previously to process experimental data of quasi-oedometric compression tests [8,10,11]. Its aim is to compute the mean radial stress and strain levels within the specimen from the records of strain gauges located on the outer surface of the cell. It also takes account of the shortening of the specimen measured with the SHPB. In order to avoid complications due to the plastification of the

cell [8,10], high-strength steel (elastic limit about 1800 MPa) was used for the present ring to insure its purely elastic behaviour. This assumption will be checked after the tests.

2.5.1. Numerical simulation of the cell alone subjected to a uniform internal pressure

Numerical simulations were performed with the cell alone in order to build relations between an internal pressure applied on its inner surface and the hoop strains in the middle of the ring and at a distance from the middle equal to 3/4 of the half-length of the ring. The idea is similar to that used in [11]. The main improvement is that the strains measured at the three axial positions are involved in the processing; leading to a more precise evaluation of stresses and strains in the specimen. Computations were performed with the finite element computer code Abaqus Implicit [18], assuming a purely elastic behaviour of the cell (Young modulus: 205 MPa, Poisson ratio: 0.29). A uniform pressure of 1000 MPa is applied on a variable height (h) (Fig. 3). This height is directly deduced from the nominal axial strain of the specimen (ε_{zz}^S) obtained from the processing of SHPB data:

$$h = h_0^S \left(1 + \bar{\varepsilon}_{zz}^S\right), \tag{1}$$

where h_0^S is the initial length of the specimen. Moreover, several simulations took account of a possible imperfect axial centring of the specimen in the ring. This could be due to an initial imperfect positioning or of the slip of the specimen inside the ring during the test. The different studied cases are summarized in Table 2. Fig. 4 shows the fields of von Mises stress and of the hoop strain obtained
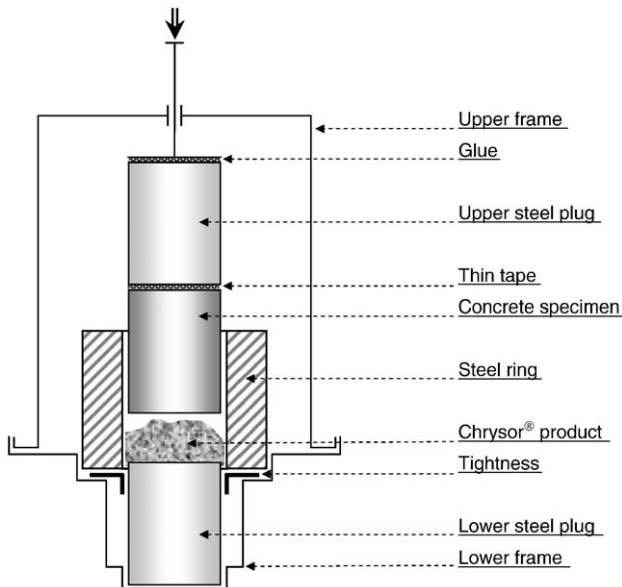

Fig. 2. Schematic of the device to set the specimen, the ring and the steel plugs.
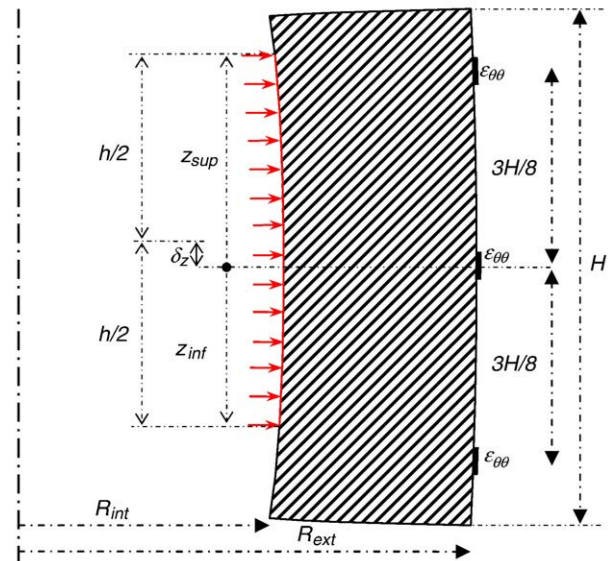

Fig. 3. Definition of the loading.

Table 2
Different loading configurations used in the numerical simulations.

h (mm)	40	40	40	38	38	38	38	36	36	36	36	34	34	34	34
δ_z (mm)	0	1	2	0	1	2	3	0	1	2	3	0	1	2	3
$\varepsilon_{\text{axial}}$ (%)	0	0	0	-5	-5	-5	-5	-10	-10	-10	-10	-15	-15	-15	-15
z_{inf} (mm)	-20	-19	-18	-19	-18	-17	-16	-18	-17	-16	-15	-17	-16	-15	-14
z_{sup} (mm)	20	21	22	19	20	21	22	18	19	20	21	17	18	19	20

for two values of (h) (40 mm and 34 mm) considering no defect of symmetry ($\delta_z = 0$). In both cases, the maximum Mises stress reaches about 2.2 GPa on the inner surface of the ring. According to these calculations, a maximum internal pressure up to 820 MPa associated with a maximum external hoop strain up to 0.25% do not induce any plastic strain in the cell.

2.5.2. Radial stress and strain levels in the specimen deduced from strain gauges G1 to G6

The results of numerical simulations are presented in Fig. 5. The problem being purely linear, hoop strains ($\varepsilon_{\theta\theta}^{(z=0)}$, $\varepsilon_{\theta\theta}^{(z=+3H/8)}$, $\varepsilon_{\theta\theta}^{(z=-3H/8)}$) are given for an applied pressure of 1 GPa and are plotted as function of (h) and (δ_z) (Fig. 5). These data provide empirical relations that are used to process the test. On the one hand, the external hoop strain on the symmetry plane ($z = 0$) is slightly depending on (h) and (δ_z). Consequently, the internal pressure is evaluated from this data ($\varepsilon_{\theta\theta}^{(z=0)}$). On the other hand, the difference between $\varepsilon_{\theta\theta}^{(z=+3H/8)}$ and $\varepsilon_{\theta\theta}^{(z=-3H/8)}$ increases quasi-linearly with the defect of symmetry (δ_z). Thus, this parameter (δ_z) may be evaluated from ($\varepsilon_{\theta\theta}^{(z=+3H/8)} - \varepsilon_{\theta\theta}^{(z=-3H/8)}$) and ($h$):

$$\delta_z = P_z(h) \times \left(\frac{\varepsilon_{\theta\theta}^{\left(z=\frac{3H}{8}\right)} - \varepsilon_{\theta\theta}^{\left(z=-\frac{3H}{8}\right)}}{\varepsilon_{\theta\theta}^{\left(z=\frac{3H}{8}\right)} + \varepsilon_{\theta\theta}^{\left(z=-\frac{3H}{8}\right)}} \right), \tag{2}$$

where $P_z(h)$ is a polynomial function of degree 1 valid for the considered cell. Similarly, a function is built to compute the internal radial stress:

$$-\frac{\sigma_{rr}^{(int)}}{\varepsilon_{\theta\theta}^{(z=0)}} = P_\sigma(h) + Q_\sigma(h) \times (\delta_z)^2, \tag{3}$$

where P_σ and Q_σ are polynomial functions of degree 2 which coefficients have been identified for the considered cell. As shown by Fig. 6, Eq. (3) allows fitting satisfactorily the numerical data in the considered range of (h) (36–40 mm) and (δ_z) (0–3 mm).The same kind of function is used for the internal hoop strains: $\varepsilon_{\theta\theta}^{(int,z=0)}$, $\varepsilon_{\theta\theta}^{\left(int,z=\frac{h_0}{2}\right)}$, $\varepsilon_{\theta\theta}^{\left(int,z=\frac{h_0}{2}\right)}$. Thus, it is possible to compute an approximate form of the average inner hoop strain ($\bar{\varepsilon}_{rr}^S$) along the specimen height ($z_{\text{inf}} \leq z \leq z_{\text{sup}}$) knowing the outer hoop strains measured on the cell and the axial strain of the specimen:

$$\bar{\varepsilon}_{rr}^S = F_1 \left(\varepsilon_{\theta\theta}^{(int,z=0)}, \varepsilon_{\theta\theta}^{\left(int,z=\frac{h_0}{2}\right)}, \varepsilon_{\theta\theta}^{\left(int,z=-\frac{h_0}{2}\right)}, \bar{\varepsilon}_{zz}^S \right), \tag{4}$$

where the function F_1 takes into account the barrelling deformation of the cell.

2.5.3. Computation of the deviatoric strength and of the compaction law from experimental data

The average radial strain of the specimen being known, the average specimen area may be also computed. The average axial stress is then:

$$\bar{\sigma}_{ZZ}^S = \frac{F_{\text{axial}}}{A_0 (1 + \bar{\varepsilon}_{rr}^S)^2}, \tag{5}$$

the value F_{axial} being deduced by the processing of SHPB data. The radial stress being known, the average deviatoric stress is:

$$\bar{\sigma}_{\text{deviatoric}}^S = \left| \bar{\sigma}_{zz}^S - \bar{\sigma}_{rr}^S \right|, \tag{6}$$

The average hydrostatic pressure and the volumetric strain are given by the formulas:

$$\bar{P}_{\text{hydrostatic}}^S = -\frac{1}{3} \left(\bar{\sigma}_{zz}^S + 2\bar{\sigma}_{rr}^S \right), \tag{7}$$

$$\bar{\varepsilon}_{\text{volumetric}}^S = (1 + \varepsilon_{zz}^S)(1 + \varepsilon_{rr}^S)^2 - 1. \tag{8}$$

Knowing the axial stress and the internal pressure, the deviatoric behaviour (i.e. the supposed evolution of the deviatoric stress versus the hydrostatic pressure) and hydrostatic behaviour (variation of the volumetric strain versus the hydrostatic pressure) can be calculated.

3. Dynamic quasi-oedometric compression tests

A series of dynamic quasi-oedometric compression tests was carried out with MB50 concrete samples and with the confining cell described above. The deviatoric behaviour and the hydrostatic behaviour were computed. A comparison between the tests will allow for an evaluation of the strain-rate effect and that of the content of water.

Two sets of MB50 concrete were used (dried and saturated specimens). The specimens were subjected to the procedure described in Section 2. First, wet and dry specimens were tested at three different dynamic loading levels. The performed tests were referenced to the measured velocity of the striker (velocity of about 6, 8.5 and 11 m/s). The mean strain rate of the corresponding tests and the mass and density of corresponding wet specimens are reported in Tables 3a and 3b. The mean strain rate of the dynamic tests is arbitrarily defined as the average value (with time) of the strain rate along the part of the curve following the peak of the strain-rate (cf. Figs. 9c and 10c).

3.1. Typical experimental data

3.1.1. Data from strain gauges

An illustration of experimental data is displayed in Fig. 7: the hoop strains recorded by gauges G1 to G6 are shown for the test performed on a wet specimen loaded by a striker with the speed of 11 m/s. Hoop strains at the middle of the cell (G1 and G2: $z = 0$) are, as expected, greater than those of the lateral gauges (G3 to G6). This is in good agreement with the results of the numerical simulation given in Section 2. Moreover, as explained in Section 2, the dissymmetry of the internal pressure can be deduced from the hoop strains recorded by the gauges located near the edges of the ring (Eq. (2)). The maximum gap with the central position was found around 0.8 mm. Now the recorded strains (Fig. 7) can be processed in order to obtain the averaged deviatoric stress (6), the hydrostatic pressure (7), and the volumetric strain (8).

3.1.2. Stresses and strains reached during one QOC test

The evolution of stresses and strains is shown for test V11a WET in Fig. 8. When the maximum load is reached (axial stress equal to
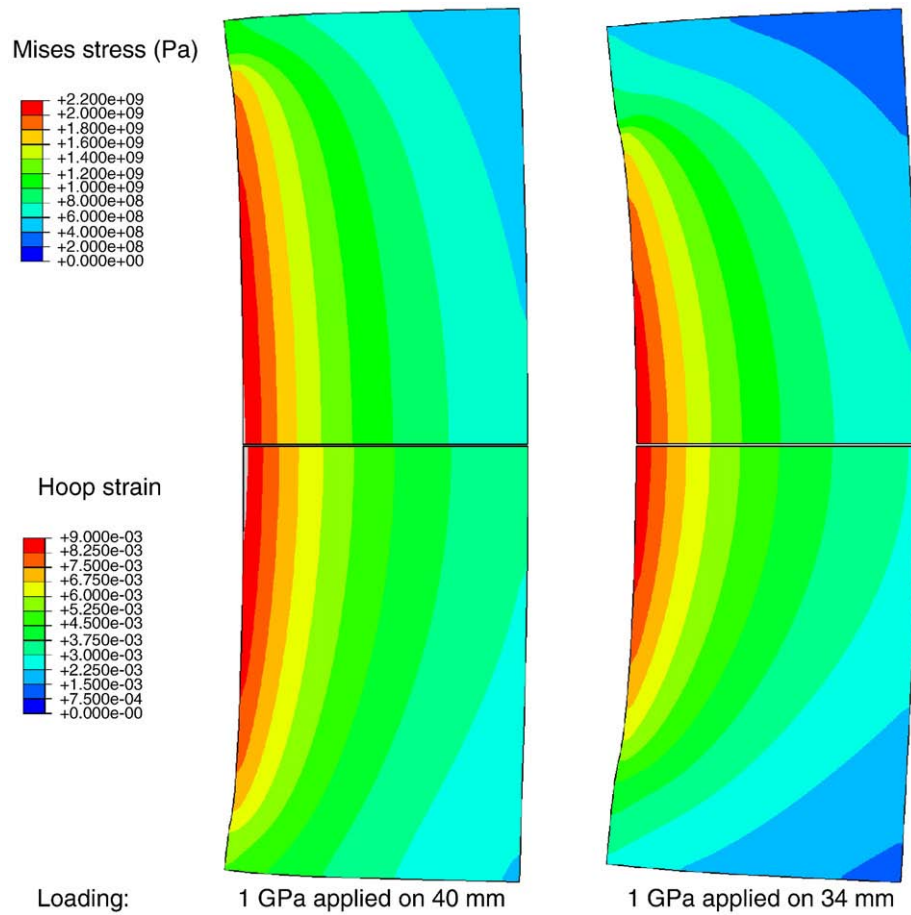
Mises stress (Pa)

```
+2.200e+09
+2.000e+09
+1.800e+09
+1.600e+09
+1.400e+09
+1.200e+09
+1.000e+09
+8.000e+08
+6.000e+08
+4.000e+08
+2.000e+08
+0.000e+00
```

Hoop strain

```
+9.000e-03
+8.250e-03
+7.500e-03
+6.750e-03
+6.000e-03
+5.250e-03
+4.500e-03
+3.750e-03
+3.000e-03
+2.250e-03
+1.500e-03
+7.500e-04
+0.000e-00
```

Loading: 1 GPa applied on 40 mm   1 GPa applied on 34 mm

Fig. 4. Numerical simulation of an elastic cell loaded by an internal pressure of 1 GPa (upper part: Mises criterion, lower part: hoop strain contours).

−1100 MPa), the hydrostatic pressure is equal to 1000 MPa. It is also observed that the lateral pressure applied by the specimen on the ring (Eq. (3)) is quite similar, in shape and in amplitude, to the axial stress.

Consequently, the deviatoric stress is almost constant during the test (in between 160 MPa and 180 MPa). The evolution of the strains is plotted on the right-hand side of Fig. 8. The axial strain reached −11%
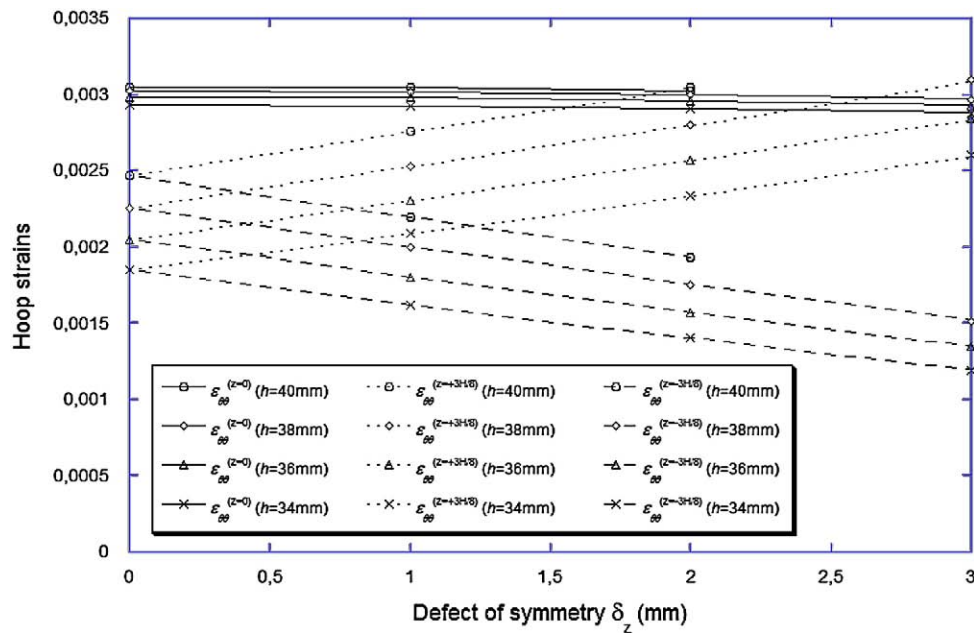

Fig. 5. External hoop strains for an internal pressure of 1 GPa versus δz (mm) considering four heights of applied pressure (40, 38, 36 and 34 mm).
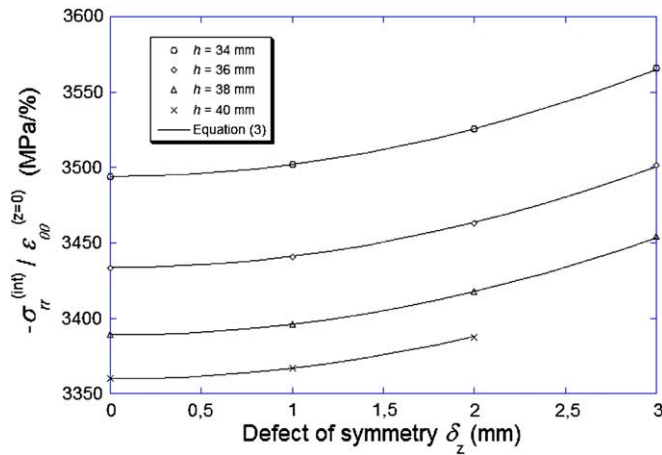
Fig. 6. Comparison between data from numerical simulations and Eq. (3).

at the end of the test. The radial strain did not exceed 0.73% so that the test may be considered as a "quasi-oedometric" test.

3.2. Results for dried specimens

The results of four dynamic tests performed on dry specimens are shown in Fig. 9. The mean strain rate of each test is given in Table 3a. It naturally increases with the striker velocity (mean strain rate of 90/s and 147/s with a velocity of the striker of 6 and 11 m/s respectively). The evolution of the hydrostatic pressure versus the volumetric strain is plotted in Fig. 9a. An almost constant bulk modulus about 6 GPa is observed in the range of hydrostatic pressure from 100 to 650 MPa for all the dynamic tests. Moreover, an important increase of the strength is observed in Fig. 9b (evolution of deviatoric stress versus hydrostatic pressure). The maximum strength reaches 600 MPa under 650 MPa of hydrostatic pressure. Finally, no significant strain rate effect is observed on both deviatoric and hydrostatic dynamic behaviours for dry specimens.

3.3. Results for saturated specimens

Dynamic tests have been performed on saturated specimens with similar striker velocities (6 m/s, 8.5 m/s and 11 m/s). The mean strain rates obtained (Table 3b) are very close to that obtained with dried specimens (in the range of 93/s to 146/s), as shown in Fig. 10. Unlike for dried specimens, the hydrostatic behaviour appears to be not linear and the bulk modulus (i.e. the slope of the curve) is increasing with the pressure level. Moreover a saturation of the strength in between 150 MPa and 240 MPa is observed. Again, no significant effect of the strain rate is observed on both deviatoric and hydrostatic dynamic behaviours.

Table 3a
Mean strain rate of tests on dry specimens and material data.

Test reference	Mean strain rate (1/s)	Wet mass (g)	Wet density (g/cm³)	Dry mass (g)	Loss in mass (%)
V6 DRY	90	59.3	2.27	55.68	6.10
V8.5a DRY	114	59.52	2.29	56.06	5.81
V8.5b DRY	120	59.44	2.27	55.88	5.99
V11 DRY	147	59.40	2.27	55.70	6.23
QS DRY — 20mn	1.1e−4	57.65	2.21	53.90	6.50

Table 3b
Mean strain rate of tests on wet specimens and material data.

Test reference	Mean strain rate (1/s)	Mass (g)	Density (g/cm³)
V6 WET	93	58.30	2.23
V8.5 WET	120	59.76	2.28
V11a WET	140	59.88	2.29
V11b WET	146	60.63	2.29
QS WET — 55 s	1.9e−3	60.20	2.305
QS WET — 22mn	1.1e−4	59.15	2.27
QS WET — 2 h	1.7e−5	59.62	2.29
QS WET — 24 h	1.5e−6	59.10	2.26

3.4. Comparison of the dynamic behaviour of dried and saturated concretes

The deviatoric and hydrostatic behaviours of two dried and two saturated specimens are plotted in Fig. 11 showing important differences. These differences have obviously to be related to the presence of free water. In particular, for a given pressure, the level of compaction is clearly greater for dried specimens. Moreover, above a pressure of 200 MPa, the evolution of the strength is quasi linear in the case of dried specimens and almost constant in that of saturated ones. Quasi-static tests will provide explanations regarding the possible role of free water.

4. Quasi-static QOC tests

4.1. Dried concrete, comparison between quasi-static and dynamic tests

A quasi-static test has been performed on a dried specimen with a constant strain rate of 0.00011/s. The hydrostatic and deviatoric behaviours are compared with dynamic results in Fig. 12. Although the loading rates differ considerably, the results are very similar, as no significant gap is observed between the two kinds of test.

4.2. Saturated concrete, comparison quasi-static/dynamic tests

Four saturated specimens have been subjected to a quasi-static loading at different loading rates (Table 3b). The specimens are named "55 s", "22 mn", "2 h", "24 h" by reference to the total duration of the test. These tests allow evaluating the sensitivity of the behaviour of saturated concrete to the strain rate over a large range of quasi-static strain rate (from of 1.9e−3 to 1.5e−6 per second). The results are plotted in Fig. 13. It is noticed that the hydrostatic behaviour found in the three slower tests ("22 mn", "2 h", and "24 h")
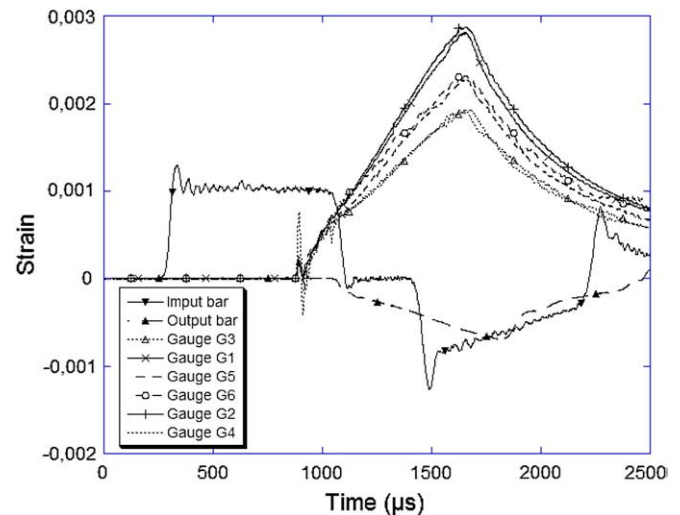

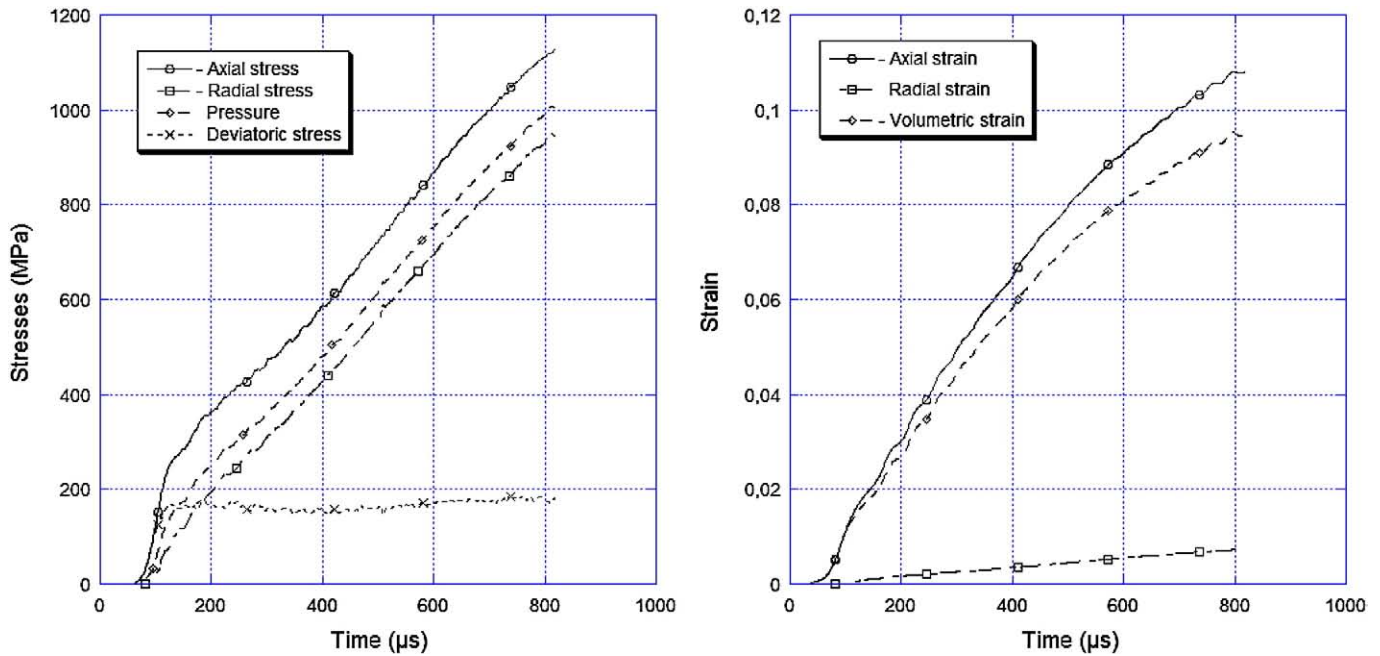**Fig. 7.** Experimental data measured in a dynamic test (V11a WET).

Fig. 8. Evolution of stresses (left) and strains (right) in a saturated specimen (V11a WET).

differ with that of the faster test ("55 s"). Moreover, a saturation of the strength is observed in the case of the faster test ("55 s") whereas a continuous increase of the strength is seen at lower loading rates (tests: "22 mn", "2 h", and "24 h"). Explanations are proposed below.

4.3. Influence of free water on the deviatoric and the hydrostatic behaviours

In order to improve the understanding of the role played by free water, the previous results (quasi-static tests, saturated specimens) are compared in Fig. 13 with that of a dynamic test (V11a WET) and that of the quasi-static test done with a dried specimen. Test "55 s" shows an evolution of the hydrostatic behaviour quite close to that of the dynamic curve "V11a WET". On the other hand, tests "22 mn", "2 h", and "24 h" show results, at the beginning (up to 8% strain) similar to those of the "QS DRY" experiment, and at the end (around 14% strain) in between those of "V11a WET" and "QS DRY". A similar trend is observed for the deviatoric behaviour. The faster QS WET test ("55 s") leads to a saturation of the strength similar to that observed in the case of dynamic tests with saturated specimens. When the loading rate decreases, the deviatoric behaviour of the tests "22 mn", "2 h", and "24 h" appears to converge towards the behaviour obtained with dried specimens (for both quasi-static and dynamic loadings). Finally, we observe that the behaviour of saturated specimens is progressively twisted from the one of "dynamic-wet" tests to the one of "QS and dynamic-dry tests" when the loading rate gradually decreases.

During quasi-static tests performed on saturated specimens, a phenomenon occurs that was neither observed in dynamic tests: an expulsion of water occurs from the gap between the plugs and the cell at both specimen sides. This phenomenon was particularly visible in slow quasi-static tests ("22 mn", "2 h", and "24 h"). It is concluded that, likely due to the high level of water-pressure, drainage is thought to occur in slow quasi-static tests. As the behaviour of wet specimens tends progressively toward that of dry specimens, one may think that there is no "chemical effect" of the free water but that its influence is mostly a question of water-pressure inside the specimen. To confirm

this hypothesis, the approximate characteristic time of drainage was computed according to the Terzaghi theory. If one considers a porous saturated material subjected to an oedometric loading (uniaxial strain) and assuming the perfect tightness boundary condition on the lateral surface and a perfect drainage boundary condition on the faces of the specimen, an analytical solution can be written (Eq. (9)) [19].

$$t_{drainage} = \frac{\gamma_w T_v H^2}{4 k E_{oedometric}} \tag{9}$$

where H is the height of specimens ($H = 40$ mm), k is the permeability coefficient of Darcy law, γ_w is the volume–weight of water ($\gamma_w = 9810$ N/m^3), $E_{oedometric}$ corresponds to the apparent elastic modulus of the skeleton in uniaxial strain (about 7 GPa according to QS DRY test) and T_v is an adimensionnal time (T_v equal 0.2 and 0.85 for respectively a drainage of 50% and 90%). The permeability coefficient of a conventional concrete was measured by SEM [28]. Two tests indicated permeability coefficients of 9e−13 and 1.4e−12 m/s, to be compared to the value of water permeability (about 1e−12 m/s) reported by Skoczylas et al. [29] in a mortar with a water by cement ratio equal to 0.5. Considering an average value of 11.5e−13 m/s, the times corresponding to 50% and 90% of drainage found for our specimen dimensions are of 97 s and 414 s ($\approx$ 7 min) respectively. These characteristic times are coherent with our hypothesis of the role of the water-pressure, as different behaviours were observed between saturated fast test ("55 s") and slow tests ("22 mn", "2 h", and "24 h"). This calculation confirms that water-pressure has probably a major influence on the confined strength and compaction law of concrete subjected to fast or dynamic loadings.

5. Discussion of the results with literature

An important feature of this work is the major role played by free water on the dynamic and static strength of concrete under confined compression − i.e. a saturation of strength for undrained wet concrete and a continuous increase of strength with dried or perfectly-drained specimens. This result may highlight the difference of behaviours previously obtained under triaxial tests [6] and quasi-oedometric
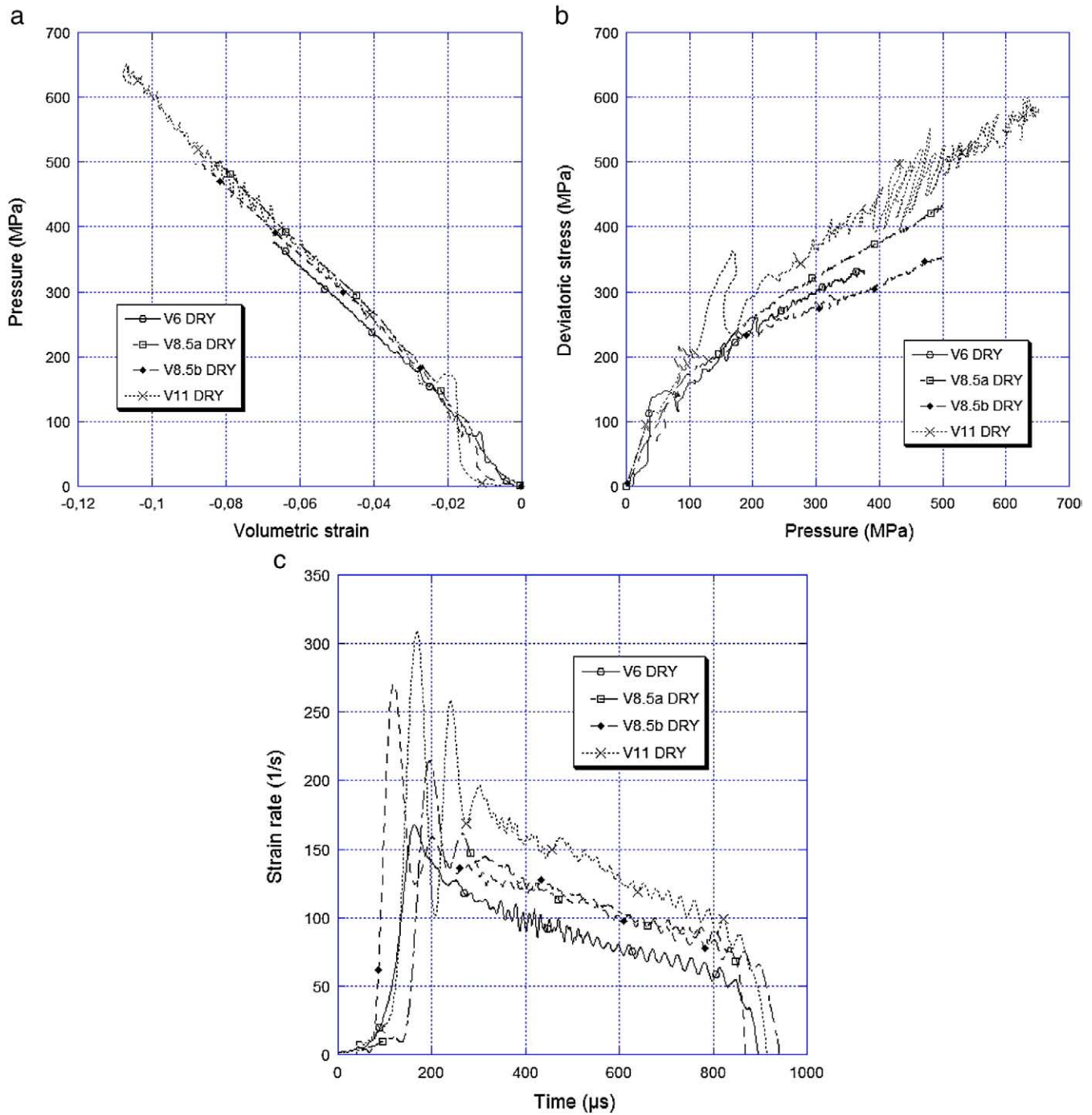
Fig. 9. Results of four dynamic tests performed on dried specimens (upper part, left: a; upper part, right: b; lower part: c).

tests [11] with a similar microconcrete. On the one hand, triaxial tests performed by [6] under hydrostatic pressures up to 1 GPa showed a saturation of strength around 500 MPa (Fig. 14). These tests were performed with wet specimens embedded in a multilayered water-tight membrane. Thus, the specimen might be considered as partially not-drained during the test. On the other hand, quasi-oedometric tests [11] were performed with specimens that were dried at an ambient temperature during several months. During these tests, the strength reached 1 GPa with a slope (stress difference/mean stress) close to one. A similar increase of the strength is observed in our work with dried specimens (Figs. 9, 14). Fig. 14 shows also a comparison of

compaction curves obtained in [11] and in the present work with dried specimen. The curves are very close to each other. The compaction curve obtained under a purely hydrostatic compression by Buzaud [6] appears to be higher than that of dried and saturated specimens. This confirms a possible influence of the loading path on the compaction behaviour (i.e. an increase of compaction process with the level of deviatoric stress, as mentioned in Section 1 [12].)

Influence of drainage conditions on the confined strength of concrete has been highlighted in previous studies under quasi-static loading. Heukamp et al. [16,17] observed no strength enhancement with pressure in undrained experiments applied to leached cement
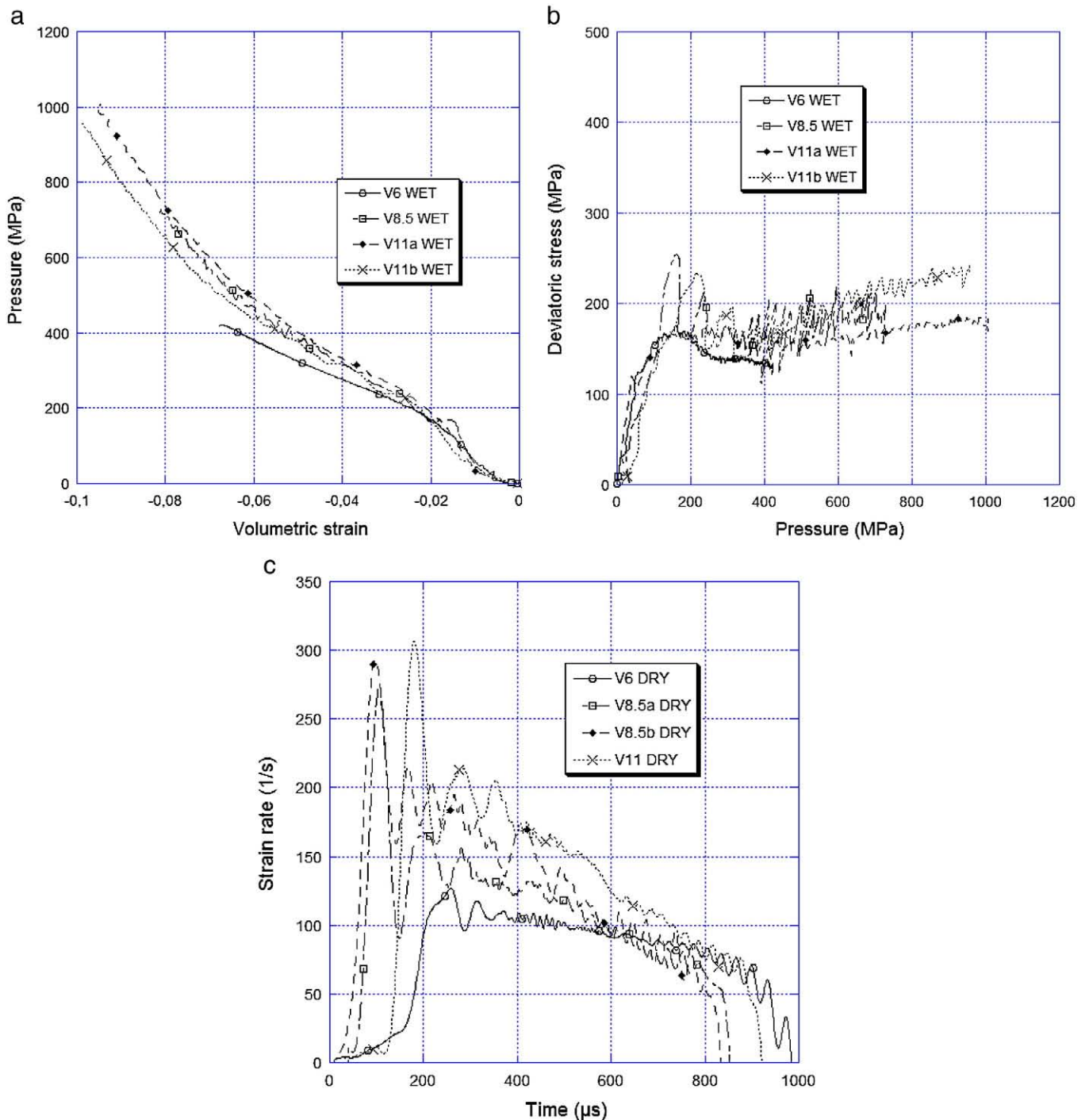
a

b

c

Fig. 10. Results of four dynamic tests performed on wet specimens (upper part, left: a; upper part, right: b; lower part: c).

paste and mortar, as a strength increase with pressure was observed in drained experiments. This result was attributed to the pore pressure that "reduces the effective confinement stress of the skeleton". More recently [31,32], tests were performed on "real" concrete specimens by means of static triaxial non-drained tests with pressure levels as high as those of the present study (about 800 MPa). The tests were performed with dried specimens and partially or completely saturated specimens. With fully saturated concrete, like for our wet-dynamic tests, a strength threshold about 200 MPa was observed whatever the pressure level reached. It is

also interesting to note, in the same reported results, that the strength of wet concretes with different saturation ratios are located at intermediate levels between the dry and the fully saturated ones. We observed a similar behaviour in our quasi-static confined tests where the varying parameter is the drainage time instead of the saturation ratio. This confirms the likely effect of pore pressure.

A more detailed analysis of the fast quasi-static ("55 s") test may be then given in the frame work of the Biot–Coussy theory of poromechanics. The total pressure $\overline{P}^{S}_{\text{hydrostatic}}$ may be expressed as a
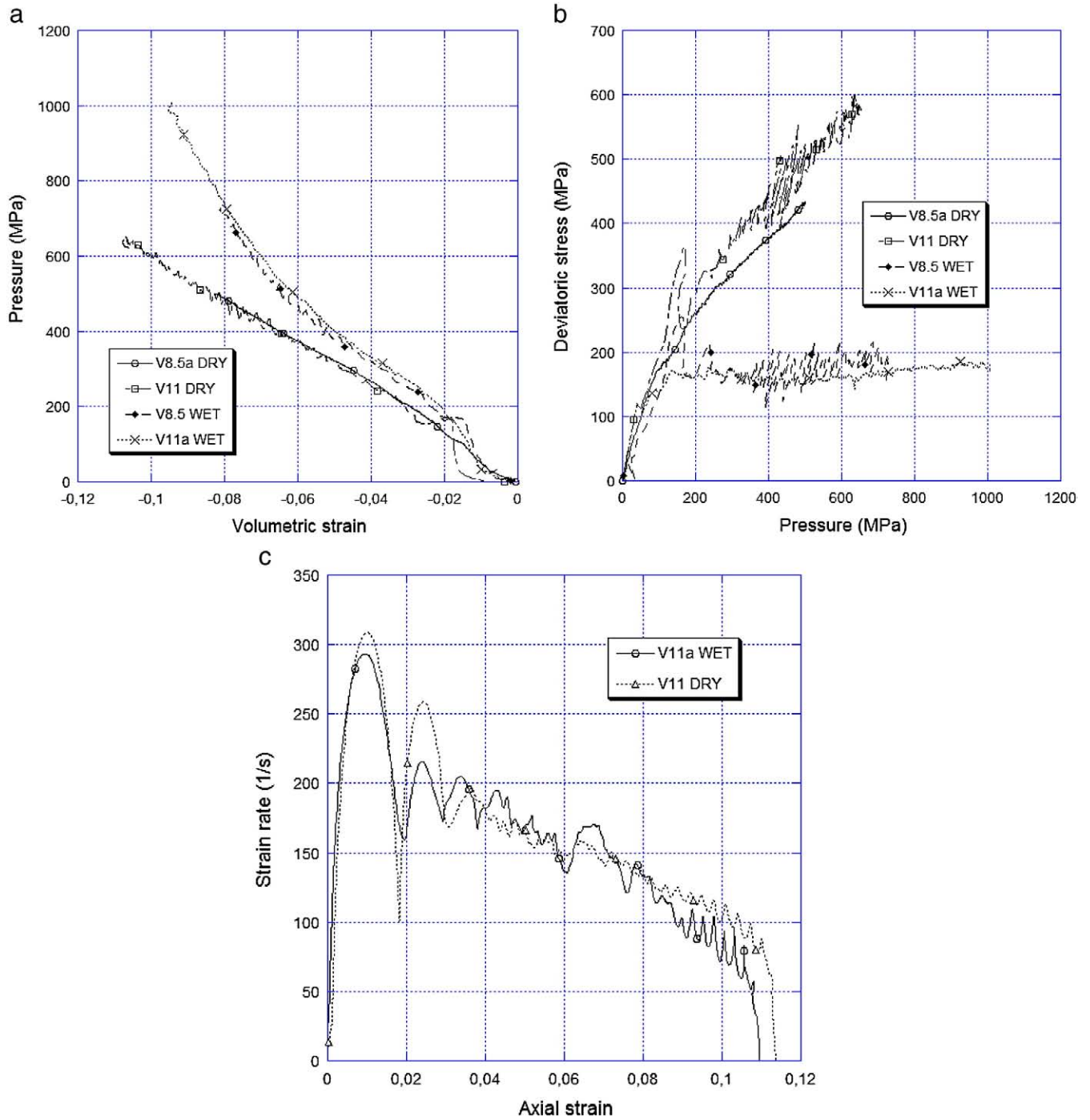
Fig. 11. Comparison of two dynamic tests performed on dried and wet specimens (upper part, left: a; upper part, right: b; lower part: c).

function of the volumetric strain $\bar{\varepsilon}^S_{\text{volumetric}}$ and the pore pressure p [7]:

$$\bar{P}^S_{\text{hydrostatic}} = -K_0 \bar{\varepsilon}^S_{\text{volumetric}} + bp \tag{10}$$

where K_0 and b denote the drained bulk modulus and the Biot coefficient, respectively. K_0 is evaluated from the quasi-static dry test ($K_0 = 4.53$ GPa) considering the range of volumetric strain involved in "55 s" test (0 to –0.09). The effective deviatoric stress $(\bar{\sigma}^S_{\text{deviatoric}})_{\text{eff}}$

may be plotted as function of the effective pressure $(\bar{P}^S_{\text{hydrostatic}})_{\text{eff}}$ considering that

$$\begin{cases} \left(\bar{P}^S_{\text{hydrostatic}}\right)_{\text{eff}} = -K_0 \bar{\varepsilon}^S_{\text{volumetric}} \\ \left(\bar{\sigma}^S_{\text{deviatoric}}\right)_{\text{eff}} = \bar{\sigma}^S_{\text{deviatoric}} \end{cases}. \tag{11}$$

When considering effective stresses (Fig. 15), results of fast saturated test are similar to those of slow saturated tests in which the pore pressure is certainly much weaker according to the analysis involving Eq. (9). It would be worth validating this approach by pore
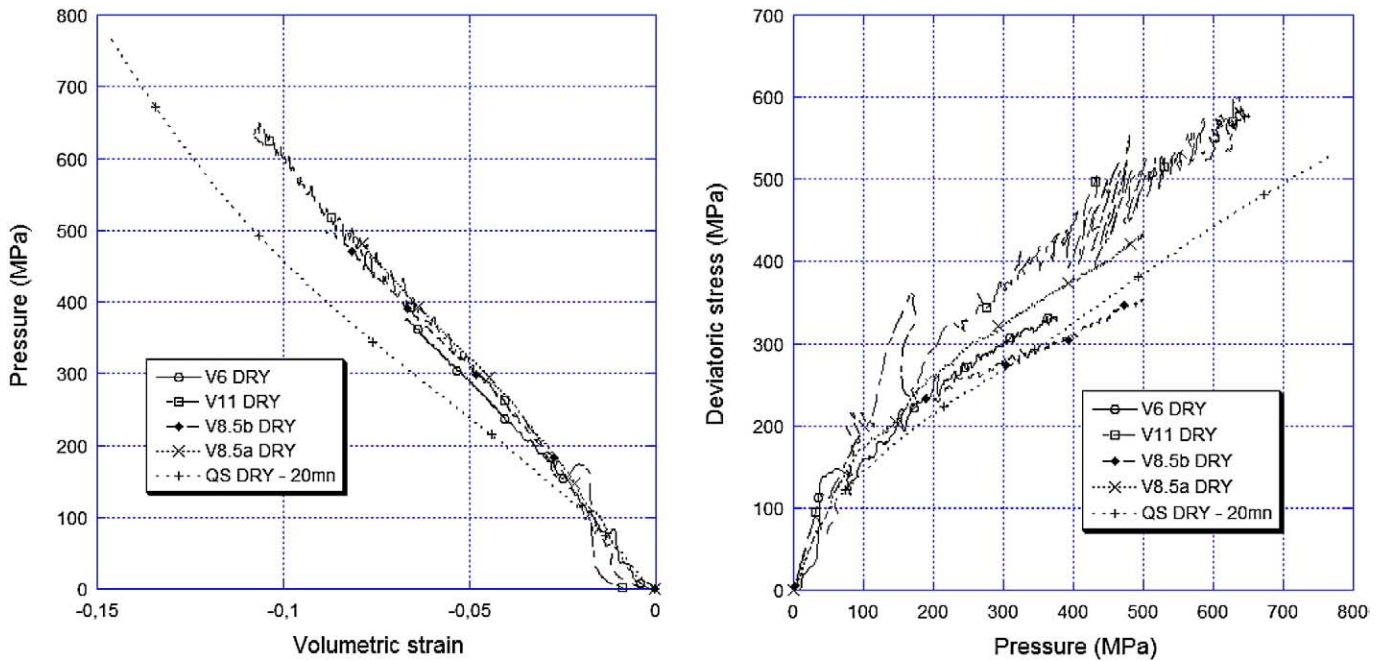
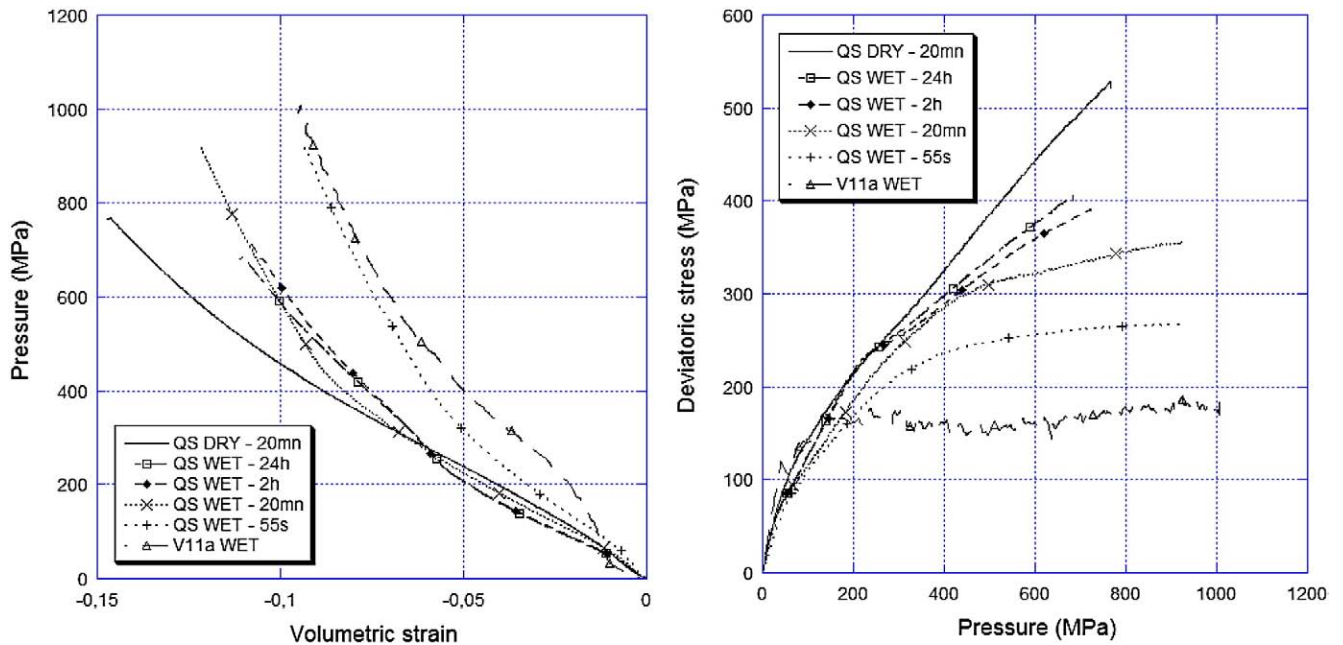Fig. 12. Quasi-static and dynamic tests performed on dried specimens.

Fig. 13. Quasi-static and dynamic tests performed on five saturated specimens and one dried specimen.

pressure measurement, but it confirms that the decrease of the strength in fast loadings might be explained, at least in part, by a reduction of the effective confining pressure applied to the skeleton [16]. However, the level of deviatoric strength observed in dynamic saturated tests (less than 200 MPa) is not properly explained through this approach. A complementary analysis might led to highlight the influence of pore pressure on the shear strength of the skeleton.

6. Conclusion

This experimental study has explored the effect of the presence of free water in concrete material, in the case of quasi-static and dynamic quasi-oedometric compression tests. The dynamic tests performed under average strain rates ($90\,s^{-1}$ till $150\,s^{-1}$) exhibited an important dissimilarity between dried and saturated specimens concerning both deviatoric and hydrostatic behaviours. A constant bulk modulus is observed for dried concretes whereas the corresponding hydrostatic behaviour of saturated specimens is non-linear. Moreover, dried concretes show a strong increase of the strength whereas water-saturated specimens exhibit an almost-perfect saturation of the strength. The quasi-static results highlighted the reason of this dissimilarity. On the one hand, no strain rate effect is observed for dried specimens On the other hand the behaviour of saturated specimens gradually tends to that of dried specimens when the loading rate decreases, as confirmed by the expulsion of water during quasi-static tests. The present experimental study shows that, partly by reducing the level of effective pressure applied to the skeleton, the pore pressure inside the concrete strongly influences the fast quasi-static and dynamic confined behaviour of concrete.
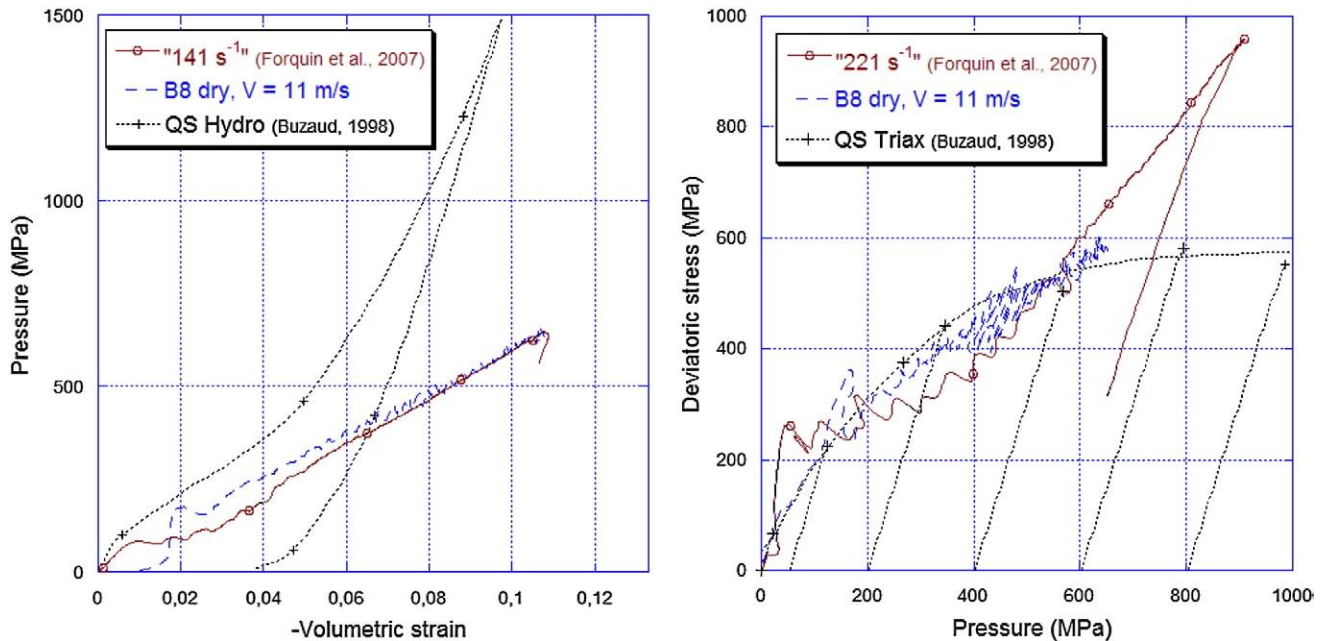

Fig. 14. Comparison of the "V11 dry" test with results from triaxial tests [6] and quasi-oedometric tests [11].

Appendix A

The waves are first shifted to bar ends, taking account of wave dispersion. Using a transient calculation with real specimen dimensions (area, length and density) and the known characteristics of the plugs, a 1-D elastic calculation with a chosen Young's modulus for concrete using the (shifted) incident wave as input data build the reflected and the transmitted wave as they would be produced by an elastic specimen. This calculation is "instantaneous". The "best" Young's modulus is then chosen (by hand) to find the best match in shape between simulated waves and the beginning of (shifted) real ones. A more precise shift is then obtained by superposing the real curves with the simulated ones. This shift is very small (a few microseconds) and has no influence on the dispersion effects. This procedure is automatically available in the software used for SHPB processing [14].

References

[1] G. Bacon, J. Carlsson, J.L. Lataillade, Evaluation of force and particle velocity at the end of a rod subjected to impact loading, J. Phys. IV 1 (1991) 395–402.
[2] Z.P. Bažant, F.C. Bishop, T.P. Chang, Confined compression tests of cement paste and concrete up to ksi, ACI J. 33 (1986) 553–560.
[3] P.W. Bridgman, Studies in Large Plastic Flow and Fracture, McGraw-Hill, New York, 1952.
[4] N. Burlion, G. Pijaudier-Cabot, N. Dahan, Expe1rimental analysis of compaction of concrete and mortar, Int. J. Numer. Anal. Methods Geomec. 25 (2001) 467–1486.
[5] Burlion N. Compaction des bétons : éléments de modélisation et caractérisation expérimentale. PhD thesis. ENS Cachan, 1997.
[6] E. Buzaud, Performances mécaniques et balistiques du microbéton MB50, DGA/Centre d'Etudes de Gramat, report, 1998.
[7] O. Coussy, Mechanics of Porous Continua, Wiley, Chichester, 1995.
[8] P. Forquin, A. Arias, R. Zaera, An experimental method of measuring the confined compression strength of geomaterials, Int. J. Solids Struct. 44 (2007) 4291–4317.
[9] P. Forquin, A. Arias, R. Zaera, Role of porosity in controlling the mechanical and impact behaviours of cement-based materials, Int. J. Impact Eng. 35 (3) (2008) 133–146.
[10] P. Forquin, A. Arias, R. Zaera, Relationship between mesostructure, mechanical behaviour and damage of cement composites under high-pressure confinement, Exp. Mech. (2008) doi:10.1007/s11340-008-9172-y.
[11] P. Forquin, G. Gary, F. Gatuingt, A testing technique for concrete under confinement at high rates of strain, Int. J. Impact Eng. 35 (6) (2008) 425–446.
[12] T. Gabet, Y. Malécot, L. Daudevielle, Triaxial behaviour of concrete under high stresses: influence of the loading path on compaction and limit states, Cem. Concr. Res. 38 (2008) 403–412.
[13] G. Gary, J.R. Klepaczko, H. Zhao, Corrections for wave dispersion and analysis of small strains with split Hopkinson bar, Proceedings of International Symposium of Impact Engineering, Vol. 1. Sendaï, Japan, 1992, pp. 73–78.
[14] Gary G. (2005) DAVID, instructions manual, Palaiseau, France. (http://www.lms.polytechnique.fr/EQUIPE/dynamique/index.html).
[15] Gatuingt, F. Prévision de la rupture des ouvrages en béton sollicités en dynamique rapide, PhD thesis, ENS Cachan, 1999.
[16] F.H. Heukamp, F.J. Ulm, J.T. Germaine, Mechanical properties of calcium-leached cement pastes: triaxial stress states and the influence of the pore pressures, Cem. Concr. Res. 31 (5) (2001) 767–774.
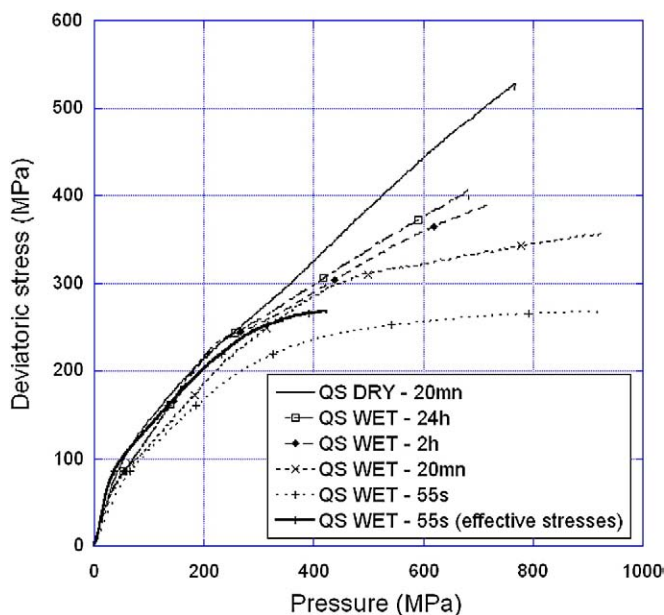
Fig. 15. Result of "QS — Wet 55 s" test expressed in effective stresses assuming perfect undrained conditions. Comparison with previous quasi-static results.

[17] F.H. Heukamp, F.J. Ulm, J.T. Germaine, Poroplastic properties of calcium-leached cement-based materials, Cem. Concr. Res. 33 (2003) 1155–1173.

[18] Hibitt H.D., Karlsson B.I., Sorensen P. Abaqus User's manuel, ABAQUS/IMPLICIT 6.1 2001.

[19] R.D. Holtz, W.D. Kovacs, An Introduction to Geotechnical Engineering, Prentice-Hall Publisher, Englewood Cliffs (USA), 1981.

[20] M.D. Kotsovos, J.B. Newman, Mathematical description of deformational behavior of concrete under generalized stress beyond ultimate strength, J. Am. Concr. Inst. ACI 77 (1980) 340–346.

[21] Q.M. Li, S.R. Reid, H.M. Wen, A.R. Telford, Local impact effects of hard missiles on concrete targets, Int. J. Impact Eng. 32 (1–4) (2005) 224–284.

[22] X. Lu, C.T. Hsu, Behavior of high strength concrete with and without steel fiber reinforcement in triaxial compression, Cem. Concr. Res. 36 (9) (2006) 1679–1685.

[23] B. Lundberg, J. Carlsson, K.G. Sundin, Analysis of elastic waves in non-uniform rods from two-point strain measurement, J. Sound Vib. 137 (3) (1990) 483–493.

[24] A. Mahboubi, A. Ajorloo, Experimental study of the mechanical behavior of plastic concrete in triaxial compression, Cement Conc. Res. 35 (2005) 412–419.

[25] R. Palaniswamy, S.P. Shah, Fracture and stress–strain relationship of concrete under triaxial compression, J. Struct. Div. ASCE ST5 (1974) 901–916.

[26] P. Rossi, J.G.M. van Mier, C. Boulay, F. le Maou, The dynamic behavior of concrete: influence of free water, materials and structures, Mater. Struct. 25 (1992) 509–514.

[27] Schmidt J.M. High pressure and high strain rate behaviour of cementitious materials: experiments and elastic/vicoplastic modelling. PhD thesis. University of Florida, 2003.

[28] SEM Service d'Expertise en Matériaux inc, Comparaison de la perméabilité à l'eau du béton compacté au rouleau (BCR) et d'un mélange de béton conventionnel, report SEM05012, 2005.

[29] F. Skoczylas, N. Burlion, I. Yurtdas, About drying effects and poro-mechanical behaviour of mortars, Cem. Concr. Compos. 29 (2007) 383–390.

[30] Toutlemonde, F. Résistance au choc de structures en béton, PhD thesis, Ecole Nationale des Ponts et Chaussées, 1994.

[31] X.H. Vu, Y. Malécot, L. Daudeville, Comportement du béton sous fort confinement : Influence du degré de saturation et du rapport Eau/Ciment, 25ème rencontre de l'AUGC, 2007, pp. 23–25, Bordeaux.

[32] X.H. Vu, Y. Malécot, L. Daudeville, E. Buzaud, Experimental analysis of concrete behavior under high confinement: effect of the saturation ratio, Int. J. Solids Struct. 46 (2009) 1105–1120.

[33] T. Warren, A. Fossum, D. Frew, Penetration into low-strength (23 MPa) concrete: target characterization and simulations, Int. J. Impact Eng. 30 (2004) 477–503.

[34] R.G. Zimmerman, Major factors affecting the multiaxial compressive strength of plain concrete, The Deformations and the Rupture of Solids Subjected to Multiaxial Stresses, Proc. of RILEM Int Symposium, Cannes, RILEM, Paris, vol. 1, 1972, pp. 257–272.

[35] J.A. Zukas, Penetration and Perforation of Solids, Impact Dynamics, Krieger Publishing Company, 1992.